Di-hydrogen contact induced lattice instabilities and structural dynamics in complex hydride perovskites

---

Schouwink, Pascal; Hagemann, Hans-Rudolf; Embs, J P; D'Anna, V; Cerny, Radovan

Di-hydrogen contact induced lattice instabilities and structural dynamics in complex hydride perovskites

P Schouwink[1], H Hagemann[2], J P Embs[3], V D'Anna[2,4] and R Černý[1]

[1] Department of Quantum Matter Physics, Laboratory of Crystallography, University of Geneva, 24 Quai Ernest-Ansermet, CH-1211 Geneva, Switzerland
[2] Department of Physical Chemistry, University of Geneva, 30 Quai Ernest-Ansermet, CH-1211 Geneva, Switzerland
[3] Laboratory for Neutron Scattering, Paul Scherrer Institut, ETH Zurich, CH-5232 Villigen, Switzerland

E-mail: pascal.schouwink@unige.ch

Abstract

The structural phase transitions occurring in a series of perovskite-type complex hydrides based on the tetrahydroborate anion BH_4^- are investigated by means of *in situ* synchrotron x-ray powder diffraction, vibrational spectroscopy, thermal methods and *ab initio* calculations in the solid state. Structural dynamics of the BH_4 anion are followed with quasi-elastic neutron scattering. We show that unexpected temperature-induced lattice instabilities in perovskite-type $ACa(BH_4)_3$ (A = K, Rb, Cs) have their origin in close hydridic di-hydrogen contacts. The rich lattice dynamics lead to coupling between internal B-H vibrations and phonons, resulting in distortions in the high-temperature polymorph that are identical in symmetry to well-known instabilities in oxide perovskites, generally condensing at lower temperatures. It is found that anion-substitution $BH_4^- \leftrightarrow X^-$ (X = Halide) can relax distortions in $ACa(BH_4)_3$ by eliminating coulomb repulsive $H^- \cdots H^-$ effects. The interesting nature of phase transition in $ACa(BH_4)_3$ enters an unexplored field of weak interactions in ceramic-like host lattices and is the principal motivation for this study. Close di-hydrogen contacts suggest new concepts to tailor crystal symmetries in complex hydride perovskites in the future.

Keywords: perovskite, hydride , quasielastic neutron scattering, phase transition

S Online supplementary data available from stacks.iop.org/JphysCM/27/265403/mmedia

(Some figures may appear in colour only in the online journal)

1. Introduction

The possibility of promoting H_2 release mechanisms by utilising close heteropolar di-hydrogen contacts between protic $H^{\delta+}$ and hydridic $H^{\delta-}$, covalently bound to nitrogen and boron atoms, respectively, has recently attracted major interest in the hydrogen storage community and is being implemented to tailor gas release-kinetics in boron–nitrogen systems under investigation [1]. While such chemical proton-hydride concepts are potentially useful to facilitate H_2-elimination, we herein

attempt to consider the question as to whether homopolar di-hydrogen contacts may also be exploited, i.e. those between atoms of the same sign charge, for instance to geometrically engineer lattice instabilities in crystal lattices, alluding to other geometrical schemes applied to generate low symmetries in solids [2–5]. To investigate this, we choose one of the simplest and best known structure types known to solid state science, the ABX_3 perovskite. Perovskite functionalities are known to be extremely sensitive to small structural distortions, and many properties adopt critical values across phase transitions, which hence play a crucial role in perovskite engineering. This concerns, for instance, electronic and magnetic transitions,

[4] Present address: Laboratoire de Chimie, ENS de Lyon, Site Jacques Monod - 46 alle d'Italie - 69364 Lyon cedex 07, France

which is impressively demonstrated by interface-design of heterostructured superlattices [6]. In this context, and on a structural level, it is of interest to produce polar-structures, which allow for polar properties, such as spontaneous polarization. Metal borohydrides often crystallize in subgroups of related isoelectronic metal oxides and chlorides, where low symmetric distortion variants are generated upon the substitution $Cl^- \leftrightarrow BH_4^-$. Possibly the most prominent structural characteristic of the perovskite type lattice is the emergence of different lattice instabilities at low temperatures due to the condensation of octahedral rotation or polar displacement modes. In turn, this signifies that crystal space group (SG) symmetry increases with temperature. A series of complex hydrides based on the tetrahydroborate anion BH_4^- and crystallizing in the ABX_3 type lattice was reported very recently [7], presenting the first genuine tunable host lattice within iono-covalent hydrides and drawing interest not only for solid state hydrogen storage but also physical properties related to heavy metals and lattice instabilities. It was found, that, on a structural level, mixed-metal borohydride perovskites undergo polymorphic transformations, where the high-temperature (*HT*) polymorph has lower space group symmetry relative to the low-temperature (*LT*) polymorph. Such a behaviour is exotic for the perovskite structure, and has to our knowledge not been described in metal-oxide or halide perovskites of very basic stoichiometry ABX_3. It is thus particularly interesting to investigate the cause of this behaviour in detail, since it is presumably owed to BH_4-specific effects not found in any other perovskite systems. The emerging high-temperature instabilities have their origin in additional structural degrees of freedom incorporated by placing the BH_4 group on the anion site of the ABX_3 lattice, enriching the structural dynamics of these compounds. Such instabilities can therefore no longer be treated as soft modes, and the concept of 'freezing' due to the lowering of thermal energy $k_B T$ is no longer appropriate. On one hand, perovskite-type borohydrides should be subject to the structure-type characteristic instabilities invoked by polar displacements and octahedral rotations. On the other hand, features specific to the borohydride anion are bound to introduce new structural phenomena. These features include the geometry of the anion, which, unlike metal oxides, halides or oxynitrides, is tetrahedral, due to the charge distribution on the BH_4 group. Beyond that, the lattice dynamics are enhanced by molecular B-H vibrations and tumbling motions (reorientations) of the molecule, which occur at relatively higher and lower energies with respect to lattice phonons. Finally, the above introduced di-hydrogen contacts, though spanning low interaction energies between approximately 2 and 120 kJ mol^{-1} [8], make up a large number of interactions per unit cell in complex hydride condensed solids, and are thus expected to participate in dominating structural behaviour, presumably interacting with lattice dynamics. The main objective of this article is to provide insight into the structural details and lattice dynamics on various time-scales governing the interesting nature of polymorphic transformations in borohydride perovskites. It is suggested that di-hydrogen contacts may become a novel tool to design crystal symmetries. In a first part the different structural transition mechanisms are discussed in the compound-series

$ACa(BH_4)_3$ (A = K, Rb, Cs) on the basis of synchrotron x-ray powder diffraction data. We choose this series of three compounds because they provide a possibility to systematically study the effect of A-cation size, which increases along the series, and results in different phase transition mechanisms. In a second part, infrared and Raman vibrational spectroscopies are employed to place the high energy molecular vibrations of the BH_4 in context with structural details and the transition behaviour. In a third part, the low energy reorientations of the BH_4 group are investigated with quasi-elastic neutron scattering and the evolution and nature of BH_4 disorder across phase transitions are discussed.

2. Experimental details

All perovskite-type metal borohydrides discussed herein were prepared by mechano-chemistry, high-energy ball-milling, in a Fritsch Pulverisette P7 planetary ball mill. 60 cycles of 2 min each, interrupted by a 5 min cooling break to prevent heating and agglomeration of powder on the walls of the milling jar, were carried out at 600 rpm. Borohydride precursors ABH_4 (A = K, Rb, Cs) were purchased at Katchem and used as received. $Ca(BH_4)_2$ was purchased at Sigma-Aldrich and $Mn(BH_4)_2$ prepared according to a similar procedure as used for $Mg(BH_4)_2$ [9]. The synthesis of $KYb(BH_4)_3$ was based on a metathesis reaction between a halide precursor $YbCl_2$ (Sigma Aldrich), $LiBH_4$ (Sigma-Aldrich) and KBH_4 (Katchem) according to $KBH_4 + 2LiBH_4 + YbCl_2 \rightarrow KYb(BH_4)_3 + 2LiCl$. A second batch of samples $ACa(BH_4)_3$ was prepared for neutron experiments using ^{11}B-enriched precursors (Katchem). *In situ* synchrotron radiation x-ray powder diffraction (SR-XPD) was performed at the Swiss-Norwegian beamlines of the European Synchrotron Radiation Facility (ESRF, Grenoble, France) and at the Swiss Light Source of the Paul Scherrer Institut (PSI, Villigen, Switzerland). Superstructures were modelled and solved in direct space using the software FOX [10] and treating the BH_4 group as a rigid body with a B-H distance of 1.13 Å. Rietveld refinements were carried out on the obtained models using TOPAS-Academic [11] treating BH_4 as a semi-rigid body with one common refined B-H distance and applying appropriate anti-bump restraints. Distortion modes were analysed using the Amplimodes [12] tool implemented on the Bilbao Crystallographic server. Hydrogen Dynamics were studied by means of quasi-elastic neutron scattering at the FOCUS beamline of the spallation source SINQ at the Paul Scherrer Institute (PSI, Villigen, Switzerland) [13, 14], at a wavelength of 4 Å. Data were converted from ToF to energy transfer and analysed using the software package DAVE [15]. The molecular vibrations of the BH_4 molecule (deformation and streching modes) were investigated with Raman and Infrared spectroscopy. Infrared spectra were collected on a Biorad Excalibur instrument (spectral resolution of 1 cm^{-1}) and Raman spectra with a 488 nm solid-state laser and a Kaiser optical Holospec monochromator equipped with a liquid-cooled CCD camera. Differential scanning calorimetry (DSC) and thermogravimetry (TGA) were performed with a Netzsch 404 F3 Pegasus apparatus under nitrogen flow. All

Table 1. Superstructures of perovskite-type borohydrides. The supercell metric is referred to a basic cubic unit cell containing one formula unit.

Compound	Space Group	Supercell	T / K
RbCa(BH$_4$)$_3$	$A2_1 22$	$\sqrt{2}/2\sqrt{2}/4$	343
CsMn(BH$_4$)$_3$	Cc	$\sqrt{6}/\sqrt{2}/\sqrt{12}$	298
CsMg(BH$_4$)$_3$	Cc	$\sqrt{6}/\sqrt{2}/\sqrt{12}$	298
KYb(BH$_4$)$_3$	$Pm2_1 b$	$\sqrt{2}/2/2\sqrt{2}$	370
BaTiO$_3$	$C222_1$	$\sqrt{6}/\sqrt{2}/\sqrt{12}$	90
ReO$_3$	$C2/c$	$\sqrt{6}/\sqrt{2}/\sqrt{12}$	298 (3 Kbar)

Note: The values are compared to related metrics found for BaTiO$_3$ [16] and ReO$_3$ [17].

sample handling was carried out under inert conditions in Ar, N$_2$ or He atmosphere. The solid state calculations which are referred to in this article have been discussed recently [7] and are not outlined again.

3. Results and discussion

3.1. Superstructures from synchrotron x-ray diffraction

The occurrence of large superstructures of commensurate modulation already for very simple compositions AB(BH$_4$)$_3$ appears to constitute a general rather than anomalous behaviour of mixed-metal perovskite-type borohydrides, and is not restricted to specific tolerance factors. For instance the values of t for RbCa(BH$_4$)$_3$, CsMn(BH$_4$)$_3$ and KYb(BH$_4$)$_3$ show quite a spread with 0.836, 0.921 and 0.817, respectively [7]. While the following discussion deals with superstructures generated during phase transitions at high temperatures, other examples have been found, where the room temperature polymorph crystallizes in a superlattice, as compared to the basic cubic perovskite aristotype unit of, e.g. STO. Representative examples of the large unit cells are listed in table 1.

Modulated structures have been reported for ternary fluoride-perovskites, where both commensurate and incommensurate modulations are generated by displacements induced by size-mismatches due to the smaller fluoride anion and its lack of polarizability. With a radius of approximately 2.03 Å, the size of the (BH$_4$)$^-$-anion, however, lies between the bromide and the iodide anion. The tendency to form superstructures (commensurately modulated) hence must be owed to properties specific to the borohydride ligand, (i) tetrahedral charge distribution and (ii) close homonuclear di-hydrogen contacts. The supercell-metric ($\sqrt{6}/\sqrt{2}/\sqrt{12}$) corresponding to both CsMn(BH$_4$)$_3$ and CsMg(BH$_4$)$_3$ is identical to that found for a nano-crystalline monoclinic high-pressure polymorph of ReO$_3$ [17] and an intermediate low-temperature modification of BaTiO$_3$ [16]. We would like to remind that x-ray powder diffraction on ball-milled complex hydrides as in this study presents working at the limits of what is attainable with synchrotron x-ray diffraction. The dominant element, hydrogen, is the weakest scatterer in the periodic table and small distortions giving rise to weak superstructure reflection can be interpreted wrongly or even missed if care is not taken. The

supercell metric ($\sqrt{6}/\sqrt{2}/\sqrt{12}$) having been reported at least twice strengthens the results of our structure solution for the respective cases. CsMn(BH$_4$)$_3$ has no subcell to the superstructure in the investigated temperature range between 100 K and its decomposition. In the Cc-phase the Mn-atom is shifted off-centre towards a square pyramidal coordination. The refinements were stabilized by a parabolic function in TOPAS, introducing a penalty on certain coordination environments and favouring a 5 + 1 coordination around the manganese centre, which resulted in improved residuals R$_{wp}$ (Rietveld plots available in Supplemental Material, figure S1–S3, available at stacks.iop.org/JphysCM/27/265403/mmedia). Though locally off-centred and hence polar, the Mn atom is nevertheless on average expected to be in the centre of the octahedron, leading to the cancellation of any spontaneous dipole moment. Orbital effects can be excluded as a possible cause of the modulation in CsMn(BH$_4$)$_3$, since the Mg-modification CsMg(BH$_4$)$_3$ adopts the exact same supercell metric. The analysis of diffuse x-ray scattering has recently identified many prototypical ferroelectrics to contain localized dipoles either in polarized nano-domains or as individual octahedra throughout the structure, already in the (on average) paraelectric phase [18–20]. In the following, we discuss the different mechanisms leading to the emergence of low-symmetric superstructures in the high-temperature polymorphs of ACa(BH$_4$)$_3$. The other perovskite-type metal borohydrides [7] have so far not been studied in such detail.

3.2. High temperature structural phase transitions

The introduced concepts lead to differing mechanisms at phase transformations in the ACa(BH$_4$)$_3$ series. This suggests that chemical pressure exerted by the A-cation impacts both on transition temperatures T_c as well as the nature of the mechanism. Therefore, it is possible that critical homopolar di-hydrogen contacts H···H correlate with the size effect controlled by the ionic radius of A. Three case studies are discussed below to illustrate the influence of A-size, comprising displacive and order-disorder transitions, as well as intermediate cases. KYb(BH$_4$)$_3$ also undergoes a high-temperature transformation to lower symmetry at 365 K (Supplemental figure S4, available at stacks.iop.org/JphysCM/27/265403/mmedia), but is not discussed here since the B-cation is not Ca.

3.2.1. KCa(BH$_4$)$_3$: atomic displacements and instabilities.
The room-temperature modification of KCa(BH$_4$)$_3$ is orthorhombic. At approximately 345 K an orthorhombic-orthorhombic transition takes place with a hysteresis of 20 K (figures 1 and 2), during which the unit cell is doubled in size. The phase transition implicates an instability, which in metal-oxides is commonly stabilized at low temperatures and corresponds to the condensation of a soft mode of symmetry $Pnma$. This is a very common zone-boundary instability in perovskites [4] implying out-of-phase octahedral rotations [21]. The low temperature polymorph LT-KCa(BH$_4$)$_3$ was modelled and refined in space group $Pba2$. The octahedral rotation pattern of this model is $a^0 a^0 c^+$, which is the characteristic tilt pattern
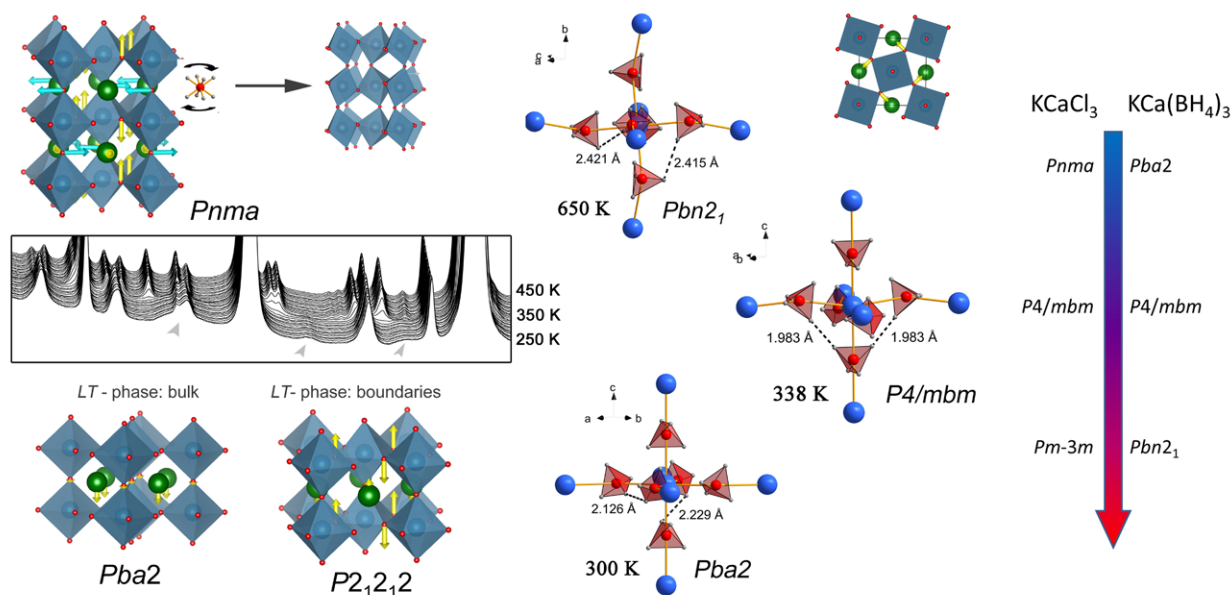
Figure 1. Relevant structural features describing both polymorphs and the transition intermediate of $KCa(BH_4)_3$. *In situ* x-ray diffraction is shown, broad features attributed to grain boundaries in the *LT*-polymorph are highlighted with grey arrows. The minim value of the H...H is given for all structural models involved in the transition. The transition sequence of $KCa(BH_4)_3$ is compared to that of the related halide $KCaCl_3$ [24] on the right.
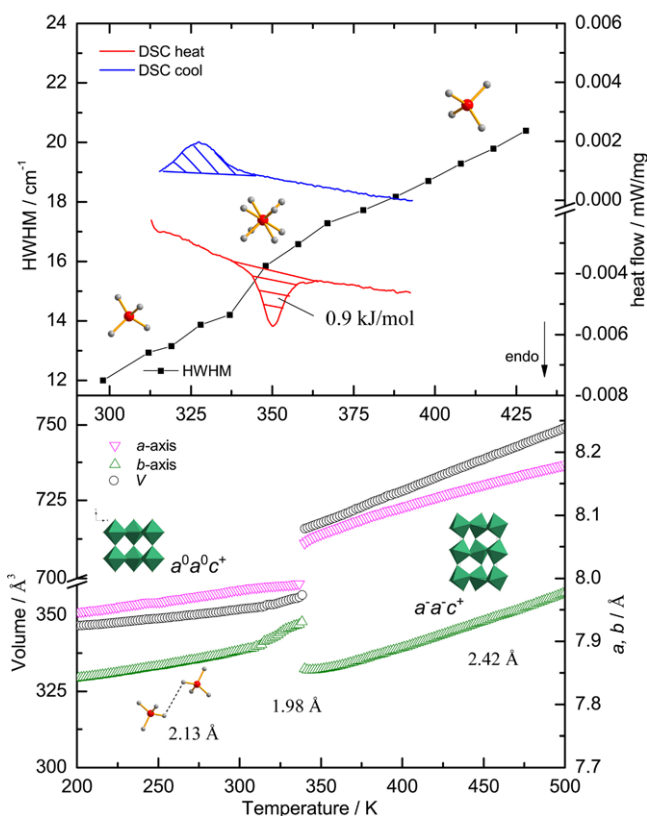
Figure 2. Heat flow and Raman bandwidth of the B-H bending mode for the transition in $KCa(BH_4)_3$ (top) along with unit cell volume and lattice parameters (bottom).

of an *R*-point instability leading to the tetragonal perovskites of space group symmetry *P4/mbm*, a 2-fold supercell to the basic cubic primitive unit. Both the loss of inversion symmetry

and deviation from tetragonality can be understood as consequences of BH_4-ordering and accompanying effects discussed below. Beyond this deviation we suppose that more severe distortions are introduced, that manifest themselves as broad subgroup reflections in the powder pattern (figure 1).

These broad reflections are present only in the low-temperature phase, and disappear upon heating across the transition, reversibly reappearing upon cooling. A number of models were developed to explain these reversible broad signals. Initially they were attributed to contributions from diffuse scattering, which is a very common phenomenon in perovskite phases, currently being investigated in many prototypical ferroic materials to solve long-standing ambiguities [19, 22, 23]. Diffuse scattering in reciprocal space arises from local order in direct space. The former has defined shapes and a specific *hkl*-dependent directionality in reciprocal space as a consequence. The broad features in the diffraction data of *LT*-$KCa(BH_4)_3$ were indexed to space group $P2_12_12$ (figure 1), conserving the lattice dimensions of the sharp Bragg signals in its supergroup *Pba*2. The broadening itself was found to be *hkl*-independent, allowing us to exclude the diffuse component. We thus attribute the broadening to genuine size effects at grain boundaries, which are marked with arrows in figure 1, and associated local distortions. It is well-known that inversion symmetry can be lifted locally by distortions arising at domain walls or interfaces in heterostructures for instance. In this view the mechano-chemical synthetic approach of the samples presented here should be kept in mind, which produces grain-aggregates of micron size, but domain sizes that are far below that. The coherence length, tantamount to the domain-size in this case, was refined using the instrumental resolution function collected on a silicon standard. The isotropic size parameter increases abruptly by a factor

Table 2. Optimized symmetries and calculated energies per unit cell of $KCa(BH_4)_3$ [7].

Input symmetry	Output symmetry	Energy (eV)
HT- Pbn2$_1$	*Pbn2*$_1$	−163.868
HT- Pbnm	*Pbnm*	−163.788
P4/ mbm	*P2*$_1$*2*$_1$*2*	−164.020
P4 bm	*Pba2*	−163.775
LT- Pbam	*P2*$_1$*2*$_1$*2*	−164.023
LT- Pba2	*Pba2*	−163.802

Note: Energies have been scaled to the number of formula units in the *LT*-phase for comparison.

of approximately 5 across the phase transition of $KCa(BH_4)_3$, from 40 nm in the *LT*-phase (considered temperature range: 100 to 345 K) to 200 nm in the *HT*-phase (considered range: 345–500 K). This provides an explanation for the growth of domains in the high-temperature polymorph, manifested in the improved peakshape, and according to our model is accompanied by strain-relaxation at the grain boundaries. The abrupt nature of the change in size precludes temperature-assisted annealing and attributes the domain-growth to the phase transition, the change in domain size is fully reversible upon cooling into the low-temperature phase. The exact reason for the low-symmetric $P2_12_12$ regions has not been found up to date. However, we recently reported solid state calculations on the different polymorphs of $KCa(BH_4)_3$ and proposed $P2_12_12$ to be the ground state of $KCa(BH_4)_3$ [7]. In this context, it is assumed that stress and strain generated in the sample during mechano-chemistry are responsible for destabilizing the ground state with respect to higher symmetries.

It is worth inspecting the calculated energies of the involved $KCa(BH_4)_3$ polymorphs optimized by periodic density function theory calculations and given in table 2. It is seen that centrosymmetric input models result in a symmetry change towards $P2_12_12$ while the polar *LT*-$KCa(BH_4)_3$ model *Pba*2, which allows to maximize H· · ·H distances, conserves its symmetry. The returned energies are lowest for output symmetries corresponding to the broad features in the diffraction pattern (figure 1). Possibly small-angle grain boundaries may be at the origin of this since they form to lower the energy of a structure. Approaching the phase transformation, figure 2 illustrates an interesting pre-transition behaviour of *LT*-$KCa(BH_4)_3$. Prior to the onset, the lattice parameters *a* and *b* evolve towards identical values and hence tetragonality, which corresponds to the *T*-dependent symmetry evolution characteristic of the lattice type.

In structurally related metal oxides, or halides such as $KCaCl_3$ [24], $CsCaCl_3$ [25] or $CsSrCl_3$ [26], the *LT*-polymorph subsequently transforms to tetragonal and then cubic symmetry (figure 1, right). The pre-transition behaviour of $KCa(BH_4)_3$ is therefore interesting, as it represents the intuitive temperature evolution of the perovskite lattice. The activation of the lattice instability *Pnma* (figure 1) in the *HT*-polymorph, however, violates this evolution. The underlying mechanism may be investigated by taking a closer look at the tetragonal transition intermediate.

Though never realized in experiment, it can be calculated by DFT, and necessarily involves one disordered BH_4-position, which is occupying a Wyckoff site higher in symmetry than the symmetry of a tetrahedron -43*m*. The transition enthalpy of 0.9(2) kJ mol^{-1} is significantly below the value of RTln2 = 2.02 kJ mol^{-1} expected for an order–disorder event (figure 2). The discrepancy may be explained by the partial activation of disorder on a specific site only. In figure 1, the shortest interatomic hydrogen-hydrogen distances between atoms pertaining to adjacent BH_4 ligands are labelled for all models relevant to the transformation and calculated in the solid state. We assume that the dominant interaction between these hydridic hydrogen atoms is of coulomb repulsive nature. Similar to the Switendick criterion for stable hydrides, these close hydridic homopolar di-hydrogen contacts therefore provide an explanation for the lattice instability. Ordered anion substituted variants $KCa(BH_4)_2Br$ and $KCa(BH_4)Br_2$, where the halide substitutes for BH_4 on the apical and equatorial sites of the CaX_6 octahedron, preserve tetragonal input symmetry during optimizations [7]. Obviously, halide substitution stabilizes the tetragonal phase. This is in good agreement with the hypothesis of repulsive di-hydrogen contacts at the origin of exotic high-temperature lattice distortions, since these close contacts no longer exist in the halide-substituted variants.

3.2.2. CsCa(BH$_4$)$_3$: order–disorder. The mechanism underlying the phase transition in $CsCa(BH_4)_3$ can be regarded as the opposite extreme to the displacive nature of $KCa(BH_4)_3$. $CsCa(BH_4)_3$ undergoes a continuous transition at 510 K without hysteresis (figure 3). The transition enthalpy of 5.5(5) kJ mol^{-1} is approximately twice the value of RTln2 for a pure order–disorder transition, where two different orientations of BH_4 are considered. The large enthalpy may thus arise from more than two different configurations. Interestingly, no superstructure reflections appear in the x-ray diffraction pattern, which does not change qualitatively across the transition. The temperature-dependence of the unit cell volume (figure 3) nevertheless reveals a smooth positive anomaly centred slightly above 500 K. The transformation mechanism therefore need not imply structural rearrangements. *LT*-$CsCa(BH_4)_3$ crystallizes in space group *Fm*−3*c* in the as-milled samples. This corresponds to the symmetry of the high-temperature modifcation of $Y(BH_4)_3$ [27]. The structure type of $Y(BH_4)_3$ is ReO_3, which is an *A*-site vacant perovskite. In its low-temperature modification the octahedral network in $Y(BH_4)_3$ is distorted in *Pa*-3. In *HT*-$Y(BH_4)_3$ 90° flips of exactly 50% of borohydride ligands have allowed to maximize H· · ·H distances, relaxing the distortion at the same time. In $CsCa(BH_4)_3$ the *A*-site is fully occupied, hence restricting the available space for the specific distortion of *LT*-$Y(BH_4)_3$. The maximization of all H· · ·H distances is possible only in the ordering scheme produced by space group *Fm*-3*c*, which we find to be the stable symmetry down to 10 K. The high-temperature polymorph is decribed by us as fully disordered *Pm*-3*m*, explaining the absence of superstructure reflections in the low-temperature phase. The ordered polymorph of $CsCa(BH_4)_3$ is an 8-fold supercell to the fully disordered one. The space-groups *Fm*-3*c* and *Pm*-3*m* are thus related by doubling of the cubic cell parameter. The relationship between the *F*-centred and the
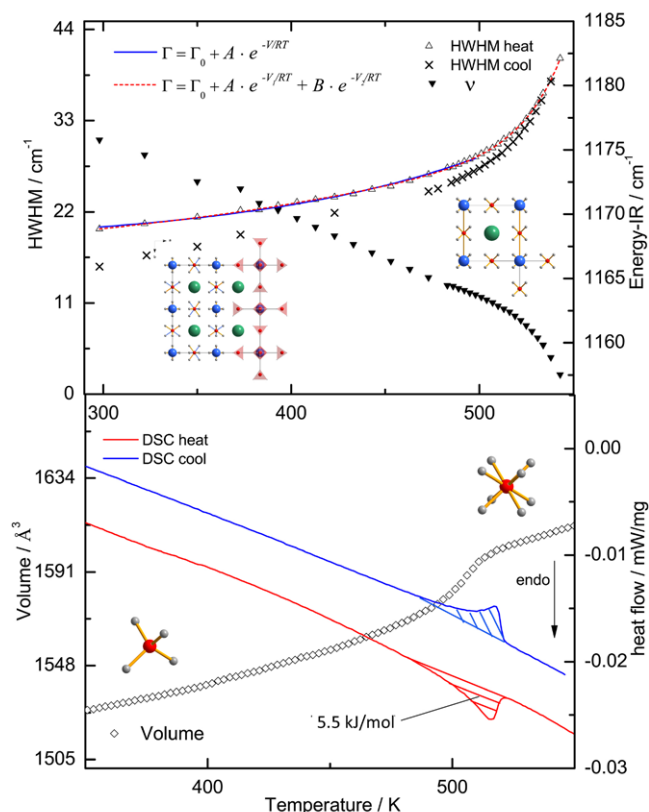
Figure 3. Bandwidth and position of the infrared-active B-H bending mode during the transformation in $CsCa(B_4)_3$ (top), structural models of the 8-fold ordered supercell Fm-$3c$ (LT) and the fully disordered Pm-$3m$ (HT) are shown next to data, as well as the fit of two different models to the evolution of HWHM. The heat flow (bottom) shows no hysteresis and the unit cell expands smoothly across the transition.

primitive cubic unit cell can account for an identical x-ray diffraction pattern, in spite of different systematic extinctions, as was the case for $Y(BH_4)_3$. The origin of unit-cell axis doubling is therefore exclusively related to the positional ordering of BH_4-groups, which occupy a disordered position $4/mm.m$ ($3d$) in the Pm-$3m$ HT-phase, and order on position $-4m.2$ ($24c$) in the Fm-$3c$ LT-phase. In contrast to $KCa(BH_4)_3$ there is hence no genuine lattice instability involved in superstructure generation.

3.2.3. RbCa(BH$_4$)$_3$: instabilities and disorder. The ionic radius of Rb^+ lies in between those of K^+ and Cs^+, and the transformation-sequence of $RbCa(BH_4)_3$ unifies atomic displacements and order–disorder mechanisms. Identical to $CsCa(BH_4)_3$, the RT-polymorph of $RbCa(BH_4)_3$ is described as cubic Fm-$3c$ (mistakenly described as P-$43m$ in [7]). Upon temperature increase, two discrete thermal events are detected, labelled **I** and **II** in figure 4, the first with a hysteresis ΔT of approximately 17 K while the second is non-hysteretic. A continuous process takes place at $T > 420$ K during which the structure evolves to cubic symmetry in the $HT3$-phase [7]. The cubic-orthorhombic transformation at 370 K, event **I** results in a 16-fold supercell metric of $HT1$-$RbCa(BH_4)_3$, space group $A2_122$, which has no precedence in the literature and is stable only in a small temperature range of
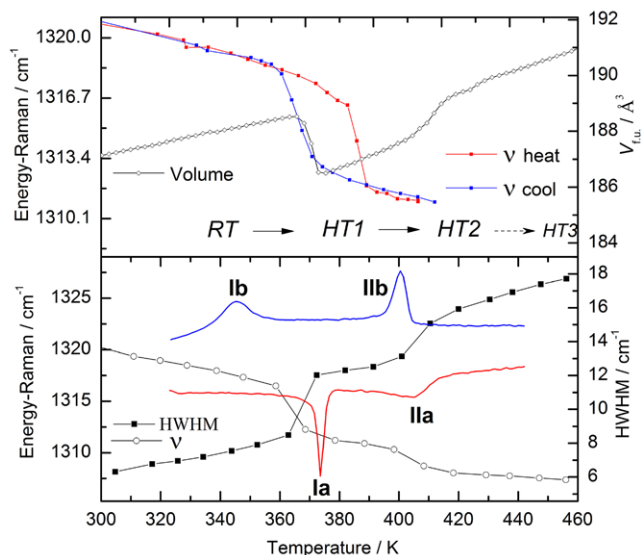
Figure 4. Band position (top and bottom) and width (bottom) of the Raman-active B-H bending vibration monitored across the phase transformations in $RbCa(BH_4)_3$. The temperature-dependent unit cell volume is shown in the upper panel. Thermal events are labelled with roman numerals (bottom).

approximately 30 K (370–400 K). The commensurate modulation in the $HT1$-polymorph is attributed to H⋅⋅⋅H interactions, and is accompanied by a negative volume anomaly of -1.2%. The subsequent orthorhombic-tetragonal and tetragonal-cubic transformations are again in agreement with the general temperature-dependency of the lattice type.

Transition enthalpies for the events **I** and **II** in figure 4, i.e. $RT \rightarrow HT1$ and $HT1 \rightarrow HT2$, are $1.3(1)$ and $1.0(1)$ kJ mol^{-1}, respectively. Interestingly, it is possible to stabilize the modulated $HT1$-phase at room temperature by substituting $Ca^{2+} \leftrightarrow Mg^{2+}$ on the B-site. Supposedly the smaller size of the Mg^{2+} cation stabilizes the displacements present in the modulation of the superstructure.

The corresponding enthalpies of partially Mg-substituted $RbCa_xMg_{1-x}(BH_4)_3$ are $0.2(1)$ and $1.0(1)$ kJ mol^{-1}, for events **I** and **II**. Thus, while the transition enthalpy of the second transition is unchanged, that of the first is a factor $\times 10$ smaller. A slight volume jump still persists in the Mg-stabilized variant [7]. This evidences that transition **I** arises mostly due to atomic rearrangements, while **II** involves disordering of BH_4 groups to some extent, which is not affected by the cation substitution. The hystereses of both transitions, namely 17 and 0 K, supports these mechanisms, and is in agreement with the hystereses of the displacive and pure order-disorder events in $KCa(BH_4)_3$ and $CsCa(BH_4)_3$.

## 3.3. Structural dynamics

The mechanisms controlling phase transitions in borohydride perovskites are closely related to the dynamics of the BH_4 complex. In perovskite-type lattices these structural dynamics of the anion provide an additional parameter to trigger and possibly control the well known lattice instabilities hosted by the lattice-type. Such structural anion dynamics comprise the
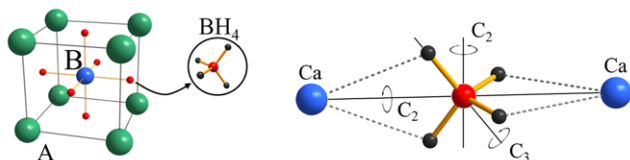
Figure 5. Schematic view of the borohydride-perovskite structure (left) and the principal axes of reorientation of the BH_4 molecule.
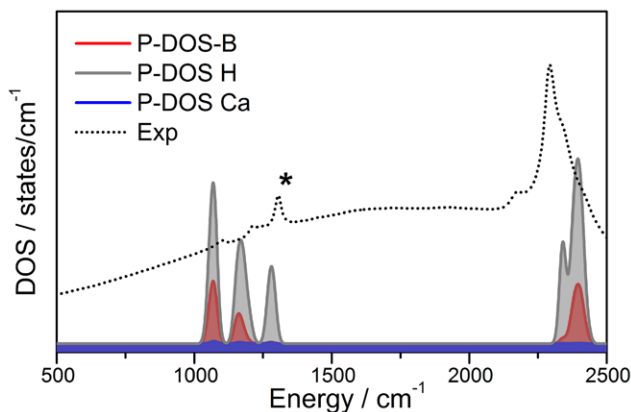
Figure 6. Partial calculated vibrational density of states P-DOS for *LT*-$KCa(BH_4)_3$ compared to the experimental Raman spectrum (dotted line). The monitored signal is marked with an asterisk.

molecular B-H stretching and bending vibrations of the BH_4 molecule as well as the low energy librations and reorientations. B-H vibrations are readily studied by vibrational spectroscopy while the much lower energy transfers of stochastic reorientations are investigated by means of quasi-elastic neutron scattering. The structural dynamics of monometallic borohydrides have been extensively investigated by vibrational spectroscopy [28–30], solid state NMR spectroscopy [31–35], inelastic x-ray scattering IXS [36], inelastic neutron scattering INS [37], QENS [38–40] and recently by molecular dynamics assisted density functional theory (MD-DFT) [41, 42]. The importance of the vibrational density of states for the stabilities of different polymorphs has also been discussed [43].

3.3.1. BH_4 vibrations. B-H bending and stretching vibrations are observed at energies of approximately 170–180 and 300 meV (1300 and 2400 cm^{-1}). The stretching vibrations are subject to strong Fermi-resonances which prevent the straightforward quantitative use of peak positions and line shapes [44]. In a perovskite-type octahedral framework, the anion is sandwiched between two *B*-cations (figure 5) in an approximately linear coordination. This situation is comparable to the anion environment in ReO_3-type $Y(BH_4)_3$. The latter compound has been studied theoretically in detail [45] and the reported phonon density of states compares well to the one obtained for $KCa(BH_4)_3$, shown in figure 6. In particular, we have identified a signature signal (figure 6) of this coordination scheme in $B(BH_4)^{n-}$ frameworks, which is sufficiently isolated in both Raman and infrared spectra as to allow for line shape analysis. Infrared as well as Raman spectra can be obtained from our own database [46].

It is interesting to note that the two lower frequency deformation modes at ca 1090 and 1180 cm^{-1} present strong contributions of the boron motions and correspond to strong IR bands, while the highest energy deformation band (around 1320 cm^{-1}) is the strongest in the Raman spectra. These features are common to all $ACa(BH_4)_3$ compounds studied here (Supplemental figures S5–S7, available at stacks.iop.org/JphysCM/27/265403/mmedia). However, it is important to note that the spectra of $KCa(BH_4)_3$ show much broader bands than those observed for the two other compounds. The positions and width (half width at half maximum HWHM) of these deformation modes (observed in both IR and Raman spectra) were monitored as a function of temperature across the high temperature phase transitions. The temperature dependent IR and Raman spectra clearly show the different phase transitions taking place. These results are illustrated in figures 2–4 as well as in the Supplemental Material (Supplemental figure S8, available at stacks.iop.org/JphysCM/27/265403/mmedia). The differences in the behaviour of HWHM are considerable between compounds $ACa(BH_4)_3$. The high temperature transformations in $KCa(BH_4)_3$ and $RbCa(BH_4)_3$ are accompanied by discrete steps in the evolution of both band position (negative step) and HWHM (positive step). The hysteresis of both discontinuities is visible in the energy of the Raman-active ν_3 bending mode for $RbCa(BH_4)_3$ (figure 4, top) and is in good agreement with the value of 17 K, determined from thermal analyses. Such a step is absent in the case of $CsCa(BH_4)_3$ (figure 3). This difference needs to be placed into context with the structural investigations on the Cs-perovskite borohydride. The corresponding results discussed above have allowed to exclude the participation of any lattice instability, hence atomic displacements, from the transition mechanism of $CsCa(BH_4)_3$. The latter is therefore best rationalized as order–disorder, as explained above. Analysis of the signature vibration in $CsCa(BH_4)_3$ in figure 3 (top) shows that both the HWHM and band position evolve smoothly and without hysteresis, which is in good agreement with the transition enthalpy shown in figure 3.

In figure 3, the evolution of the linewidth as a function of temperature can be described by an exponential relation

$$\Gamma(\omega, T) = a + b \cdot e^{-\frac{V}{RT}} \quad (1)$$

where *V* is the barrier of reorientational motion in the solid [47]. This relation accounts for an anharmonic coupling of a reorientational motion to the deformation mode considered. This behaviour has been studied previously in the alkali borohydrides [28, 29]. The corresponding results are included in table 3. The maximum value for a barrier of reorientation can also be estimated [29] from the position of the highest energy librational mode according to the relation (I is the moment of inertia of the BH_4^- ion)

$$V = \frac{\pi^2 \cdot I \cdot \nu^2}{2} \left(1 + \frac{h}{2 \cdot \pi^2 \cdot I \cdot \nu} \right)^2 \quad (2)$$

At room temperature, the highest energy librational bands are observed in the Raman spectra of $RbCa(BH_4)_3$ (427 cm^{-1}, HWHM 26) and $CsCa(BH_4)_3$ (433 cm^{-1}, HWHM 17, Supplemental figure S7, available at stacks.iop.org/

Table 3. Activation energies (in kJ mol^{-1}) of different jump motions determined from QENS in borohydride perovskites of the series ACa(BH$_4$)$_3$.

	2-site	3-site	2 ⊗ 3-site (slow, fast)	4-site	1-step (IR)	2-step (IR)
KCa(BH$_4$)$_3$ *LT*	13(1)	15(1)	18.4(7),12(1)		9(2)	
HT	5.4(9)	10(1)	6.8(7),12(1)		3(3)	
Rba(BH$_4$)$_3$ *LT*	16(2)	16(2)		21(2)	18(4)	8(3),59(4)
*HT*1	19.7(9)	21(3)			73(30)	
*HT*2	27(2)	15(2)	10.3(6),3.7(3)			
CsCa(BH$_4$)$_3$ *LT*	5.7(6) **IR** 18(1)	9(1)			18(1)	7(2),56(9)
HT	81(7) **IR** 76(14)	81(4)		101(14)	76(14)	

Note: The values obtained from infrared (IR) spectroscopy on CsCa(BH$_4$)$_3$ are included for comparison.

JphysCM/27/265403/mmedia). Assuming a B–H bond length of 1.22 Å, the obtained maximum values are 33.4 and 33.9 kJ mol^{-1}, respectively, which is in reasonable agreement with the value of 42 kJ mol^{-1} determined theoretically for α-Y(BH$_4$)$_3$ [45]. Two useful conclusions are deduced from the investigations on B–H vibrations. (1) The participation of genuine lattice instabilities involving atomic displacements is traceable by means of simple spectroscopic experiments, following characteristic signals, and is manifested in discrete jumps of peak parameters. (2) A certain extent of coupling must exist between the Pv-lattice instabilities commonly active in metal oxide perovskites and the molecular vibrations of BH$_4$, whose strength cannot be further identified here. Such an interaction between phonons and normal modes of the anion, occurring at considerably higher energies, may be tested in future as a means of tailoring perovskite crystal symmetries.

3.3.2. BH$_4$ reorientations. Unlike phonons, reorientational motions (tumbling) of the BH$_4$ group are not directly accessible by vibrational spectroscopy. Such motions are not collective and occur at very low energy transfers (10^{-9} eV) around zero energy transfer. This range of energy transfer is accessible with quasi-elastic neutron spectroscopy (QENS), which probes stochastic motions that lead to broadening of the elastic line if the timescale they occur in is accessible by the instrumental setup. In the following we present the first QENS measurements performed on mixed-metal borohydrides. The measured quantitiy in QENS is the total incoherent scattering function $S^{\mathrm{inc}}(Q, \omega)$ [48], which is expressed as the convolution of the instrumental resolution function $R(Q, \omega)$ with the elastic line $\delta(\omega)$ and the Lorentzian functions $L(\Gamma_i, \omega)$ which model the quasielastic broadening.

$$S^{\mathrm{inc}}(Q, \omega) = R(Q, \omega) \otimes \left[A_0(Q)\delta(\omega) + \sum_i A_i(Q)L(\Gamma_i, \omega) \right] \tag{3}$$

The bandwidth Γ_i of the quasielastic signal is related to the residence times of hydrogen atoms corresponding to different reorientation mechanims.

$$L_i(\omega) = \frac{1}{\pi} \frac{1/\tau_i}{(1/\tau_i)^2 + \omega^2} \tag{4}$$

The weight of the Lorentzian functions is called the quasielastic incoherent structure factor $A_i(Q)$. The elastic incoherent structure factor $A_0(Q)$ (EISF) is a measurable quantity obtained from the integrated elastic and quasielastic intensities $I_{\mathrm{el}}(Q)$ and $I_{\mathrm{qel}}(Q)$. Its Q-dependency can be used to trace different mechanisms implying a different number of sites accessible to the hydrogen atoms.

$$A_0(Q) = \frac{I_{\mathrm{el}}(Q)}{I_{\mathrm{el}}(Q) + I_{\mathrm{qel}}(Q)} \tag{5}$$

These models are referred to as *n*-site jump models, where *n* is the number of sites occupied during jump motions.

The different extents of order and disorder in perovskite borohydrides were investigated for ACa(BH$_4$)$_3$, with the aim of evaluating the structural dynamics in the low and high-temperature phases, and to provide evidence or counter-evidence for the models established from careful crystallographic analysis discussed in the section above. The borohydride anion can be treated in an analogous way to the isostructural ammonium (NH$_4$)$^+$ cation, which is a classical example of a solid rotor [49]. The alkali-borohydrides have been studied in detail by quasi-elastic neutron scattering and different jump models have successfully been applied to the low- and high-temperature phases [38, 39, 50]. A double-cation borohydride has so far not been studied with QENS. In the perovskite-type structure, the anion-position, in this case occupied by BH$_4$, is approximately linearly coordinated by *B*-cations (figure 5). This is a comparable situation to that found in the polymorphs of Mg(BH$_4$)$_2$, albeit in a very different underlying lattice. A recent combined QENS-DFT study deals with the thermally activated reorientations of BH$_4$ in Mg(BH$_4$)$_2$ [51]. The authors determine activation energies of 39 and 76 meV for jumps around the 2-fold (C$_2$) and 3-fold (C$_3$) axes, respectively. Furthermore they report how the measured disorder is activated in a site-specific manner. As opposed to the NaCl-type alkali-borohydrides the linear coordination rationally suggests at least two different energy barriers, due to the lower symmetry of the occupied boron position. For an ordered compound the principal expected reorientation axes that comply with the symmetry of a tetrahedron are schematically shown in figure 5 (right). It is seen that during reorientations around the two different 2-fold axes and the 3-fold axis a different number of *B*-H bonding interactions (where *B* is the *B*-site cation, *not* boron) needs to be broken, which explains the different activation energies E$_a$ for the respective motion. Soloninin *et al* recently reported activation energies for the perovskite-related compound Y(BH$_4$)$_3$ [32]. Unsurprisingly, they determined two main processes, the slower process being
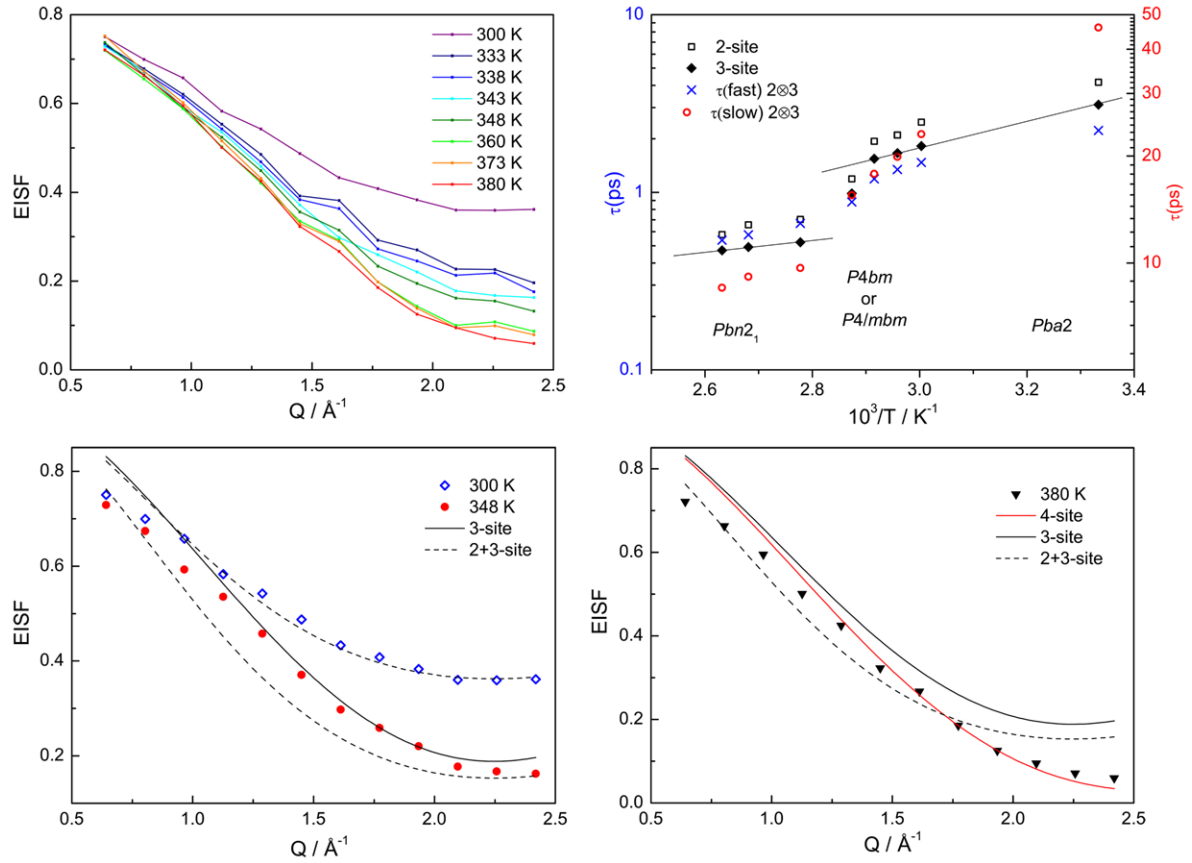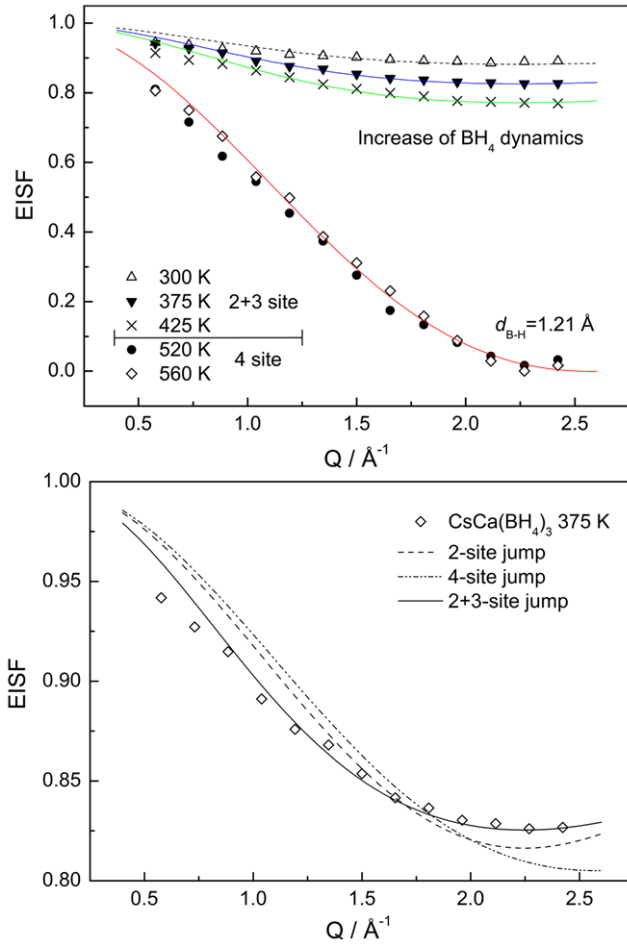
Figure 7. Summarized results from QENS for KCa(BH$_4$)$_3$, clockwise from top, left: temperature-dependent EISF, residence times for different polymorphs and jump models, EISF for *LT*-KCa(BH$_4$)$_3$ at 300 K and at the transition point of 348 K, EISF for *HT*-KCa(BH$_4$)$_3$ at 380 K. Different model-dependent fits are shown for both polymorphs.

characterized by E_a = 337 meV, the fast one by a broad distribution centered around E_a = 200 meV. The model dependant fits of Lorentzians to the quasielastic line of all datasets discussed in the following did not show any significant Q-dependency of the broadening, demonstrating that the line-broadening arises from localized hydrogen motions, not from range effects [48].

3.3.3. KCa(BH$_4$)$_3$. A question that QENS investigations were expected to answer is the nature of BH$_4$ disorder in the tetragonal transition intermediate, which is not realized in experiment but approached prior to the critical temperature T_c (figure 2). It was shown above that the common R instability is activated across the phase transition in the high temperature polymorph, introducing an additional octahedral tilt which is absent in *LT*-KCa(BH$_4$)$_3$ and proceeds via partial disorder of axial BH$_4$ groups linking in *c*-direction (figure 1) [7]. Structural x-ray investigations do not allow to draw any conclusions concerning the polarity of this disorder, and hence the correct space group of the tetragonal intermediate. To model BH$_4$-reorientations in KCa(BH$_4$)$_3$) at the transition a jump model needs to be considered which accounts for the symmetry of the Wyckoff site occupied by the boron atom. For instance, a 2-site jump model involving 180° reorientations around the 2-fold axis (figure 5) cannot model disorder. Disorder can, for instance, be achieved by 90° reorientations around
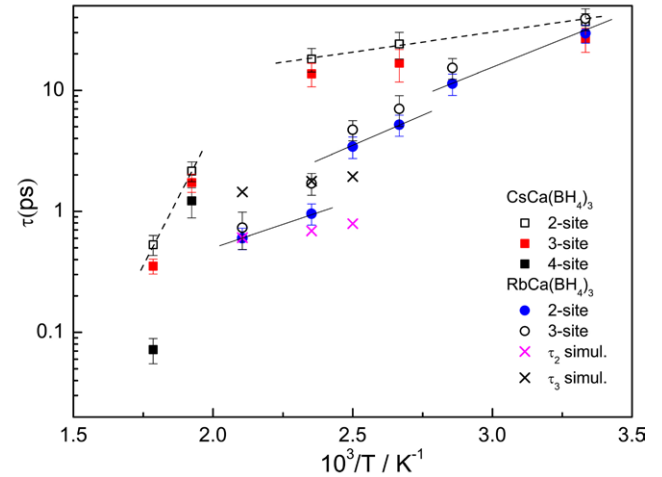
the same axis (4-site) or by 120° jumps around C$_3$ (3-site). In principle, polar disorder around a C$_3$ axis of the tetrahedron BH$_4$ (figure 5) in a 3-site jump model [48] may be separated from non-polar disorder, which can be described by 90° jumps around the C$_2$ axes in a 4-site jump model. The jump distance between symmetrically equivalent hydrogen positions is different in the respective models and can be refined from fits to the experimental EISF. Both the EISF and the residence times are reported for KCa(BH$_4$)$_3$ in figure 7. X-ray diffraction and structural optimizations suggest that disorder is localized on the BH$_4$ group bridging octahedra in the direction of the *c*-axis, which then promotes the stabilization of the *R*-instability. To account for this site-selective disorder the EISF was modified to allow for fractional disordering. The temperature-dependent EISF is shown for KCa(BH$_4$)$_3$ in figure 7 (top left). Clearly, disorder is activated gradually, and its extent levels out at 360 K, which is slightly above the structural transition (figure 2. This implies that, on the timescale of reorientational motions, BH$_4$ groups occupying positions belonging to the same Wyckoff site become inequivalent. Selective (site-specific) activation of disorder has previously been reported for the β-phase of Mg(BH$_4$)$_2$ [51]. Also for perovskite-related Y(BH$_4$)$_3$ solid state NMR studies have shown that BH$_4$ become dynamically inequivalent in spite of occupying the same Wyckoff site [32]. At 380 K, the disorder in *HT*-KCa(BH$_4$)$_3$ is best described by a 4-site model, implying 90° jumps around the C$_2$ axes (figure 7,

Figure 8. Summarized results from QENS for $CsCa(BH_4)_3$. The gradual increase of structural dynamics is shown in the upper panel. The value for the B-H distance was retrieved from a fit of a 4-site model to data collected at 520 K. The lower panel shows clear preference for the 2 + 3-site jump model in the stability field of LT-$CsCa(BH_4)_3$.

Figure 9. Residence times determined for different jump models for $CsCa(BH_4)_3$ and $RbCa(BH_4)_3$. Solid and dashed lines are guides to the eye, showing the stability field of different temperature-polymorphs.

bottom right). Data collected in the transition regime, at 348 K, suggest that the mechanism of reorientation is different from both the *LT*- and *HT*-regime. Figure 7 (bottom left) shows the corresponding Q-dependency of the EISF. The data point 348 K is located between two linear regimes describing the residence times (figure 7, top right). According to these measurements a polar disorder of the BH_4 groups involved in the transformation is more likely, i.e. implying jumps around the C_3 axes. The phase transition is also clearly visible on the residence times, which undergo a discontinuity to lower values. Arrhenius fits to the *HT*- and *LT*-data show that the activation energy decreases, which is consistent with the increase in thermal energy in the *HT*-phase.

3.3.4. $CsCa(BH_4)_3$. The order-disorder transformation predisposes $CsCa(BH_4)_3$ to be a useful model system for QENS interpretations on mixed-metal borohydrides. In figure 8 the EISFs are shown at different temperatures and compared to the discussed jump models. The structural dynamics are gradually activated in the low temperature polymorph, and the measured EISF is described quite well by a convolution

of 2- and 3-site jumps. In the disordered high temperature phase the mechanism changes to 4-site jumps, in agreement with crystallographic site symmetry of the boron position, which increases from $-4m.2$ in the *Fm-3c LT*-polymorph to $4/mm.m$ in the *Pm-3m HT*-polymorph. It can be seen in figure 8 that full disorder is reached after the transition, visible on the identical Q-dependency of datasets collected at 520 and 560 K. These data are of sufficient quality to refine the B-H distance (calculated from the jump distance), which converges at 1.21 Å, in perfect agreement with the refined B-H length reported by neutron diffraction studies on borohydrides. Two aspects however need to be addressed in this case. Firstly, the model-dependent fits of the convoluted $2 \otimes 3$ model to $S^{inc}(Q, \omega)$ do not provide reproducibly stable results. Hereby the 'slow' mechanism tends to refine to residence times close to or even above 100 ps, which is outside the upper limit of the time window accessible by FOCUS at a wavelength of 4 Å. This could suggest a very high energy barrier for the slow motion, which may originate from the relatively larger chemical pressure exerted by the larger Cs^+ cation. To access these motions future experiments may be performed at higher wavelengths, increasing the resolution around the quasi-elastic line. The residence times in table 3 are thus listed only for the fast mechanism, obtained for both the 2- and 3-site models (figure 9).

The second aspect which requires careful consideration lies in the increase of the activation energy in the high temperature phase. This is not expected but agrees well with energy barriers determined from Raman and IR measurements (table 3). In parallel to these studies solid state NMR investigations have been carried out (to be published elsewhere) and the results show that the ^1H and ^1B NMR line width drops to very low values at $T > 530$ K, which can only be explained by the onset of a translational diffusion process involving BH_4 groups. Such processes are very slow and occur on the time-scale of micro- to nanoseconds, and certainly are not observable with quasi-elastic scattering, however may influence the
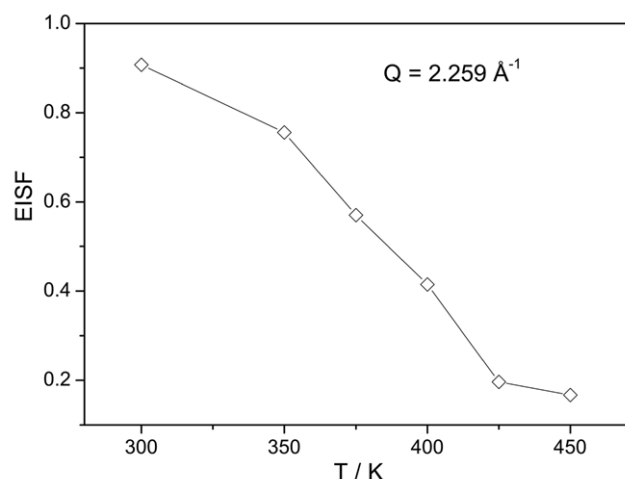
Figure 10. Qualitative behaviour of the EISF at constant Q and as a function of temperature for RCa(BH$_4$)$_3$.

accuracy of such results. The discontinuity in residence times of CsCa(BH$_4$)$_3$ between 425 and 520 K (figure 9) presumably arises from insufficient sampling in temperature.

3.3.5. RbCa(BH$_4$)$_3$. The quasi-elastic scattering of RbCa(BH$_4$)$_3$ shows similar features to that of the previous *A*Ca(BH$_4$)$_3$. As an intermediate case involving both disorder and atomic displacements, the present quasielastic scattering results on RbCa(BH$_4$)$_3$ do not allow to draw firm conclusions, given the complexity of the structural transition sequence. Qualitatively, the temperature-dependency of the EISF is plotted in figure 10 for a constant momentum transfer of 2.259 Å^{-1}. Figure 10 suggests 3 different regimes located at approximately 300–350 K, 375–425 and 425–450 K, within the investigated temperature range. The slope of the EISF does not vary any further between 425–450 K, which indicates that the maximum number of borohydride groups compliant with the symmetry of the given structural model have been dynamically activated at these temperatures. This is in excellent agreement with structural, thermal and vibrational data discussed in the previous sections and shown in figure 4, and correspond to the *RT*-phase and polymorphs *HT*1 and *HT*2.

4. Conclusions

We have herein investigated structural dynamics and phase transformation mechanims in mixed-metal borohydride perovskites. It is suggested that lattice instabilities in borohydride perovskites are generated by a weak coupling between phonons and molecular vibrations, deduced from the discontinuity of peak profile parameters extracted from Raman- and infrared-active B-H bending vibrations occurring at the temperatures of polymorphic transformations. Quasi-elastic neutron scattering furthermore shows that the reorientation mechanism of low energy tumbling motions of the BH$_4$ group experiences changes across the phase transformation in all cases of *A*Ca(BH$_4$)$_3$. Related to these findings are close homopolar di-hydrogen contacts, which are assumed to play

a crucial role in their repulsive nature to stabilize the counter-intuitive lattice instabilities at higher temperatures, whereas the common symmetry evolution of perovskite-type materials has its low symmetric polymorph on the low temperature side of the phase diagram. Such findings are highly relevant as they provide means to develop new tools to tailor perovskite symmetries, based on effects specific to the borohydride group, structural dynamics and weak molecular interactions, which are not attainable with other anions used in functional perovskite design.

Acknowledgments

References

[1] Jepsen L H, Ley M B, Lee Y S, Cho Y W, Dornheim M, Jensen J O, Filinchuk Y, Joergensen J E, Besenbacher F and Jensen T R 2014 *Mater. Today* **17** 129–35
[2] Benedek N A and Fennie C J 2011 *Phys. Rev. Lett.* **106** 107204
[3] Benedek N A, Mulder A T and Fennie C J 2012 *J. Solid State Chem.* **195** 11–20
[4] Benedek N A and Fennie C J 2013 *J. Phys. Chem.* C **117** 13339–49
[5] García-Castro A C, Spaldin N A, Romero A H and Bousquet E 2014 *Phys. Rev.* B **89** 104107
[6] Zubko P, Gariglio S, Gabay M, Ghosez P and Triscone J M 2011 *Annu. Rev. Condens. Matter Phys.* **2** 141–65
[7] Schouwink P, Ley M B, Tissot A, Hagemann H, Jensen T R, Smrčok L and Černý R 2014 *Nat. Commun.* **5** 5706
[8] Echeverría J, Aullon G, Danovich D, Shaik S and Alvarez S 2011 *Nat. Chem.* **3** 323–30
[9] Schouwink P, D'Anna V, Ley M B, Lawson Daku L M, Richter B, Jensen T R, Hagemann H and Cerny R 2012 *J. Phys. Chem.* C **116** 10829–40
[10] Favre-Nicolin V and Černý R 2002 *J. Appl. Cryst.* **35** 734–43
[11] Coelho A Topas-academic; www.topas-academic.net
[12] Perez-Mato J M, Orobengoa D and Aroyo M I 2010 *Acta. Crystallogr.* **66** 558–90
[13] Mesota J, Janssen S, Holitzner L and Hempelmann R 1996 *J. Neutron Res.* **3** 293–310
[14] Janßen S, Mesota J, Holitzner L, Furrer A and Hempelmann R 1997 *Phys. B: Condens. Matter* 234–6 1174–6
[15] www.ncnr.nist.gov/dave
[16] Ogata Y, Tsuda K, Akishige Y and Tanaka M 2004 *Acta Crystallogr.* **60** 525–31
[17] Biswas K, Muthu D V S, Sood A K, Kruger M B, Chen B and Rao C N R 2007 *J. Phys.: Condens. Matter* **19** 436214
[18] Chapman B D, Stern E A, Han S W, Cross J O, Seidler G T, Gavrilyatchenko V, Vedrinskii R V and Kraizman V L 2005 *Phys. Rev.* B **71** 020102
[19] Tagantsev A K *et al* 2013 *Nat. Commun.* **4** 1–8
[20] Zhang Q, Cagin T and Goddard W A 2006 *Proc. Natl Acad. Sci.* **103** 14695–700
[21] Glazer A M 1972 *Acta Crystallogr.* **28** 3384–92
[22] Bosak A, Chernyshov D, Vakhrushev S and Krisch M 2012 *Acta Crystallogr.* **68** 117–23

[23] Ganesh P, Cockayne E, Ahart M, Cohen R E, Burton B, Hemley R J, Ren Y, Yang W and Ye Z G 2010 *Phys. Rev. B* **81** 144102

[24] Seifert H J, Fink H, Thiel G and Uebach J 1985 *Z. Anorg. Allg. Chem.* **520** 151–9

[25] Vaills Y, Buzar J, Gibaud A and Launay C 1986 *Solid State Commun.* **60** 139–41

[26] Fink H and Seifert H J 1980 *Z. Anorg. Allg. Chem.* **466** 87–96

[27] Frommen C, Aliouane N, Deledda S, Fonnelp J. E, Grove H, Lieutenant K, Llamas-Jansa I, Sartori S, Sørby M H and Hauback B C 2010 *J. Alloys Compd.* **496** 710–6

[28] Hagemann H, Filinchuk Y, Chernyshov D and van Beek W 2009 *Phase Transit.* **82** 344–55

[29] Hagemann H, Gomes S, Renaudin G and Yvon K 2004 *J. Alloys Compd.* **363** 129–32

[30] Reed D and Book D 2011 *Curr. Opin. Solid State Mater. Sci.* **15** 62–72

[31] Soloninin A V, Babanova O A, Skripov A V, Hagemann H, Richter B, Jensen T R and Filinchuk Y 2012 *J. Phys. Chem. C* **116** 4913–20

[32] Soloninin A V, Skripov A V, Yan Y and Remhof A 2013 *J. Alloys Compd.* **555** 209–12

[33] Soloninin A V, Babanova O A, Medvedev E Y, Skripov A V, Matsuo M and Orimo S-i 2014 *J. Phys. Chem. C* **118** 14805–12

[34] Skripov A V, Soloninin A V, Babanova O A, Hagemann H and Filinchuk Y 2010 *J. Phys. Chem. C* **114** 12370–4

[35] Skripov A V, Babanova O A, Soloninin A V, Stavila V, Verdal N, Udovic T J and Rush J J 2013 *J. Phys. Chem. C* **117** 25961–8

[36] Chernyshov D, Bosak A, Dmitriev V, Filinchuk Y and Hagemann H 2008 *Phys. Rev. B* **78** 172104

[37] Parker S F 2010 *Coord. Chem. Rev.* **254** 215–34

[38] Remhof A, Lodziana Z, Martelli P, Friedrichs O, Züttel A, Skripov A V, Embs J P and Strässle T 2010 *Phys. Rev. B* **81** 214304

[39] Remhof A, Gremaud R, Buchter F, Lodziana Z, Embs Jan P, Ramirez-Cuesta Timmy A J, Borgschulte A and Züttel A 2010 *Z. Phys. Chem.* **224** 263–78

[40] Udovic T J, Verdal N, Rush J J, De Vries D J, Hartman M R, Vajo J J, Gross A F and Skripov A V 2013 *J. Alloys Compd.* **580** S47 –S50

[41] Aeberhard P C, Refson K and David W I F 2013 *Phys. Chem. Chem. Phys.* **15** 8081–7

[42] Bernstein N, Johannes M D and Hoang K 2013 *Phys. Rev. B* **88** 220102

[43] Borgschulte A *et al* 2011 *Phys. Rev. B* **83** 024102

[44] Carbonnière P and Hagemann H 2006 *J. Phys. Chem. A* **110** 9927–33

[45] Lee Y S, Shim J H and Cho Y W 2010 *J. Phys. Chem. C* **114** 12833–7

[46] www.unige.ch/sciences/chifi/?ftirdb.html

[47] Bator G, Jakubas R and Baran J 2001 *Vib. Spectrosc.* **25** 101–13

[48] Bee M 1988 *Quasielastic Neutron Scattering, Principles and Applications in Solid State Chemistry, Biology and Materials Science* (Boca Raton, FL: CRC Press)

[49] Lechner R E, Badurek G, Dianoux A J, Hervet H and Volino F 1980 *J. Chem. Phys.* **73** 934–9

[50] Remhof A, Lodziana Z, Buchter F, Martelli P, Pendolino F, Friedrichs O, Züttel A and Embs J P 2009 *J. Phys. Chem. C* **113** 16834–7

[51] Blanchard D *et al* 2012 *J. Phys. Chem. C* **116** 2013–23